NASA Technical Memorandum 85857

Solution of Poisson Equations for Three-Dimensional Grid Generations

K. Fujii

October 1983

National Aeronautics and
Space Administration

NASA Technical Memorandum 85857

Solution of Poisson Equations for Three-Dimensional Grid Generations

K. Fujii, Ames Research Center, Moffett Field, California

National Aeronautics and
Space Administration

Ames Research Center
Moffett Field, California 94035

SUMMARY

A method for generating three-dimensional, finite-difference grids about complicated geometries by using Poisson equations is developed. The inhomogeneous terms are automatically chosen such that orthogonality and spacing restrictions at the body surface are satisfied. Spherical variables are used to avoid the axis singularity, and an alternating-direction-implicit (ADI) solution scheme is used to accelerate the computations. Computed results are presented that show the capability of the present method. Since most of the results presented in this paper have been used as grids for flow-field computations, this is indicative that the present method is a useful tool for generating three-dimensional grids about complicated geometries.

INTRODUCTION

In recent years, the development of techniques for generating curvilinear coordinates has received considerable attention because one of the most important requirements in making finite-difference computations of a flow field involves properly locating the nodal points in the flow field (ref. 1). For two-dimensional-flow computations, highly sophisticated grids have been obtained through a variety of grid-generation techniques, such as conformal mappings, algebraic constructions, and partial differential equation solutions. Among these, grid-generation schemes based on solution of the Poisson equations are popular and have been widely used (refs. 2-4). In this method, the coordinates of grid points in the physical domain are computed as a solution of a set of Poisson equations. The source terms appearing in the equations, which work as forcing functions, control the grid size or shape or both near the boundaries. Well-formulated automatic grid-control techniques have been developed for two-dimensional problems, and versatile program codes, such as NASA's GRAPE code (ref. 4) developed by Sorenson, are available and have been used successfully for many flow-field computations (refs. 5-7).

The development of grid-generation techniques for three dimensions somewhat lags the development of techniques for two dimensions. However, the recent rapid progress of high-speed computers makes it possible to perform even three-dimensional Navier-Stokes computations, and, hence, three-dimensional grid generation has become the key factor for flow-field computations over complex geometries. During the past few years, several papers have been written on this subject (refs. 8-10). So far as the elliptic partial differential grid-generation techniques are concerned, the essential idea is the same as that of two dimensions, although the actual formulation is much more complicated.

The present paper adopts the idea of the two-dimensional code GRAPE and extends it to three dimensions. Since the warped spherical coordinates are adequate for the three-dimensional flow-field computations, the focus is on constructing such grids. There are two unique features in the present paper: the use of the spherical coordinate variables as independent unknowns and the use of the alternating-direction-implicit (ADI) scheme as a solution method. The use of the spherical variables

removes the axis-singularity problem. The efficiency of the ADI scheme in solving the Laplacian-type equations is well known. The constraints of the surface orthogonality and the arc-length control are imposed as source terms appearing in the right-hand side of the equations to be solved. Details of the formulations and the solution, as well as computed grid examples, are presented in the following sections.

The author wishes to express his gratitude to Mr. J. O. Bridgeman, who furnished his ADI solution code, and to Dr. P. Kutler and Mr. R. L. Sorenson for their valuable suggestions during the course of this study.

BASIC EQUATIONS AND SOLUTION PROCEDURE

Although a warped spherical grid is one of the most efficient systems from a computational viewpoint, generating such a grid using partial differential equations is made difficult because of the trouble associated with the axis singularity. Steger (private communication) pointed out that one way to overcome this problem is to solve the Cartesian-type Poisson equations with spherical unknown variables. According to his suggestion, the mapping between the physical space (ρ,θ,ϕ) and the computational space (ξ,η,ζ) satisfies the following equations (see fig. 1):

$$\left.\begin{aligned} \xi_{\rho\rho} + \xi_{\theta\theta} + \xi_{\phi\phi} &= P(\rho,\theta,\phi) \\ \eta_{\rho\rho} + \eta_{\theta\theta} + \eta_{\phi\phi} &= Q(\rho,\theta,\phi) \\ \zeta_{\rho\rho} + \zeta_{\theta\theta} + \zeta_{\phi\phi} &= R(\rho,\theta,\phi) \end{aligned}\right\} \tag{1}$$

The left-hand sides do not correspond to a true Laplacian operator in spherical coordinates. Equation (1), however, satisfies the maximum principle and generates a smoothly varying grid. Interchanging the dependent and independent variables in equation (1) results in the following nonlinear equation:

$$C^{\xi\xi}\vec{\gamma}_{\xi\xi} + C^{\eta\eta}\vec{\gamma}_{\eta\eta} + C^{\zeta\zeta}\vec{\gamma}_{\zeta\zeta} + 2(C^{\xi\eta}\vec{\gamma}_{\xi\eta} + C^{\eta\zeta}\vec{\gamma}_{\eta\zeta} + C^{\zeta\xi}\vec{\gamma}_{\zeta\xi}) = -J^2(P\vec{\gamma}_{\xi} + Q\vec{\gamma}_{\eta} + R\vec{\gamma}_{\zeta}) \tag{2}$$

where

$$\vec{\gamma} = \begin{bmatrix} \rho \\ \theta \\ \phi \end{bmatrix}$$

$$C^{\xi\xi} = J^2(\nabla\xi \cdot \nabla\xi)$$

$$C^{\eta\eta} = J^2(\nabla\eta \cdot \nabla\eta)$$

$$C^{\zeta\zeta} = J^2(\nabla\zeta \cdot \nabla\zeta)$$

$$\nabla\xi = (\vec{\gamma}_{\eta} \times \vec{\gamma}_{\zeta})/J$$

$$\nabla\eta = (\vec{\gamma}_{\zeta} \times \vec{\gamma}_{\xi})/J$$

$$\Delta\zeta = (\vec{\gamma}_{\xi} \times \vec{\gamma}_{\eta})/J$$

$$J = \partial(\rho,\theta,\phi)/\partial(\xi,\eta,\zeta)$$

Source terms P, Q, and R which appear in the right-hand side of equation (2) are determined during the solution process such that the converged solution satisfies (1) the orthogonality of the grid at the body surface and (2) the specified grid

spacing adjacent to the body in the ζ-direction. The conditions for grid orthogonality at the body surface are

$$\nabla\xi \cdot \nabla\zeta = 0 \quad \text{at the body surface} \tag{3a}$$

$$\nabla\eta \cdot \nabla\zeta = 0 \quad \text{at the body surface} \tag{3b}$$

These two conditions indicate that the vector normal to the ξ = constant plane and the vector normal to η = constant plane are orthogonal to the vector normal to ζ = constant plane. The orthogonality conditions used here are in a different form from those of reference 10, but the results are identical. The third condition for determining the source terms is control of the grid spacing:

$$\vec{S}_\zeta \cdot \vec{S}_\zeta = S_s^2 \tag{3c}$$

where S_s is the arc length of the ζ-direction grid adjacent to the body surface. The procedure for determining P, Q, and R from these conditions is described as follows.

Equations (3a) and (3b) are rewittten as

$$c_\rho^\xi c_\rho^\zeta + \frac{1}{\rho^2} c_\theta^\xi c_\theta^\zeta + \frac{1}{\rho^2 \sin^2\theta} c_\phi^\xi c_\phi^\zeta = 0 \quad \text{at the body surface} \tag{4a}$$

$$c_\rho^\eta c_\rho^\zeta + \frac{1}{\rho^2} c_\theta^\eta c_\theta^\zeta + \frac{1}{\rho^2 \sin^2\theta} c_\phi^\eta c_\phi^\zeta = 0 \quad \text{at the body surface} \tag{4b}$$

By using θ_ζ, ϕ_ζ, and ρ_ζ, these equations are re-expressed as

$$\left(-\phi_\eta c_\rho^\zeta + \frac{1}{\rho^2 \sin^2\theta} \rho_\eta c_\phi^\zeta\right)\theta_\zeta + \left(\theta_\eta c_\rho^\zeta - \frac{1}{\rho^2} \rho_\eta c_\theta^\zeta\right)\phi_\zeta + \left(\frac{1}{\rho^2} \phi_\eta c_\theta^\zeta - \frac{1}{\rho^2 \sin^2\theta} \theta_\eta c_\phi^\zeta\right)\rho_\zeta = 0 \tag{5a}$$

$$\left(-\phi_\xi c_\rho^\zeta + \frac{1}{\rho^2 \sin^2\theta} \rho_\xi c_\phi^\zeta\right)\theta_\zeta + \left(\theta_\xi c_\rho^\zeta - \frac{1}{\rho^2} \rho_\xi c_\theta^\zeta\right)\phi_\zeta + \left(\frac{1}{\rho^2} \phi_\xi c_\theta^\zeta - \frac{1}{\rho^2 \sin^2\theta} \theta_\xi c_\phi^\zeta\right)\rho_\zeta = 0 \tag{5b}$$

The relationship between the (ρ,θ,ϕ) coordinates and the (x,y,z) coordinates introduces the following relation:

$$\left.\begin{aligned} x_\zeta &= (\sin\theta\cos\phi)\rho_\zeta + (\rho\cos\theta\cos\phi)\theta_\zeta + (-\rho\sin\theta\sin\phi)\phi_\zeta \\ y_\zeta &= (\sin\theta\sin\phi)\rho_\zeta + (\rho\cos\theta\sin\phi)\theta_\zeta + (\rho\sin\theta\cos\phi)\phi_\zeta \\ z_\zeta &= (\cos\theta)\rho_\zeta + (-\rho\sin\theta)\theta_\zeta \end{aligned}\right\} \tag{6}$$

Thus, the third constraint, equation (3c), can be expressed as

$$\begin{aligned} &[(\sin\theta\cos\phi)\rho_\zeta + (\rho\cos\theta\cos\phi)\theta_\zeta + (-\rho\sin\theta\sin\phi)\phi_\zeta]^2 \\ &+ [(\sin\theta\sin\phi)\rho_\zeta + (\rho\cos\theta\sin\phi)\theta_\zeta + (\rho\sin\theta\cos\phi)\phi_\zeta]^2 \\ &+ [(\cos\theta)\rho_\zeta + (-\rho\sin\theta)\theta_\zeta]^2 = S_s^2 \end{aligned} \tag{7}$$

Now, equations (5a), (5b), and (7) can be solved for ρ_ζ, θ_ζ, and ϕ_ζ. Practically, solving equations (5a) and (5b) for θ_ζ and ϕ_ζ and inserting them into equation (7) results in a quadratic equation for ρ_ζ, which is easy to solve.[1] Since every coefficient depends on the body shape only, these equations can be solved a priori and desirable ρ_ζ, θ_ζ, and ϕ_ζ are obtained before starting the solution process of equation (2).

The source terms are assumed to have the following forms:

$$\left.\begin{aligned} P &= P_1(\xi,\eta)e^{-a_1\zeta} \\ Q &= Q_1(\xi,\eta)e^{-b_1\zeta} \\ R &= R_1(\xi,\eta)e^{-c_1\zeta} \end{aligned}\right\} \tag{8}$$

Equation (4) indicates that P, Q, and R decay exponentially in the ζ-direction. Parameters a_1, b_1, and c_1 control these decay rates. By assuming equation (4), source terms in the computational volume are all determined, once source terms at the body surface (P_1, Q_1, and R_1) are determined.

Solving equation (2) for P, Q, and R results in the following equations:

$$\left.\begin{aligned} P &= -\frac{1}{J}\left[\frac{\tilde{F}(\rho)C_\rho^\xi + \tilde{F}(\theta)C_\theta^\xi + \tilde{F}(\phi)C_\phi^\xi}{J^2}\right] \\ Q &= -\frac{1}{J}\left[\frac{\tilde{F}(\rho)C_\rho^\eta + \tilde{F}(\theta)C_\theta^\eta + \tilde{F}(\phi)C_\phi^\eta}{J^2}\right] \\ R &= -\frac{1}{J}\left[\frac{\tilde{F}(\rho)C_\rho^\zeta + \tilde{F}(\theta)C_\theta^\zeta + \tilde{F}(\phi)C_\phi^\zeta}{J^2}\right] \end{aligned}\right\} \tag{9}$$

where

$$\tilde{F}(\rho) = C^{\xi\xi}\rho_{\xi\xi} + C^{\eta\eta}\rho_{\eta\eta} + C^{\zeta\zeta}\rho_{\zeta\zeta} + 2(C^{\xi\eta}\rho_{\xi\eta} + C^{\eta\zeta}\rho_{\eta\zeta} + C^{\zeta\xi}\rho_{\zeta\xi})$$

$$\tilde{F}(\theta) = C^{\xi\xi}\theta_{\xi\xi} + C^{\eta\eta}\theta_{\eta\eta} + C^{\zeta\zeta}\theta_{\zeta\zeta} + 2(C^{\xi\eta}\theta_{\xi\eta} + C^{\eta\zeta}\theta_{\eta\zeta} + C^{\zeta\xi}\theta_{\zeta\xi})$$

$$\tilde{F}(\phi) = C^{\xi\xi}\phi_{\xi\xi} + C^{\eta\eta}\phi_{\eta\eta} + C^{\zeta\zeta}\phi_{\zeta\zeta} + 2(C^{\xi\eta}\phi_{\xi\eta} + C^{\eta\zeta}\phi_{\eta\zeta} + C^{\zeta\xi}\phi_{\zeta\xi})$$

By evaluating equation (5) at the body surface along with equation (4), the following relations can be deduced:

---

[1]Since only one solution of the quadratic equation has meaning, it is necessary to choose the appropriate one. For all the cases presented in this paper, the solution with a plus sign is chosen. However, it should be carefully chosen in general.

$$\left.\begin{aligned} P_1 &= -\frac{1}{J}\left[\frac{\tilde{F}(\rho)C_\rho^\xi + \tilde{F}(\theta)C_\theta^\xi + \tilde{F}(\phi)C_\phi^\xi}{J^2}\right]_{\zeta=0} \\ Q_1 &= -\frac{1}{J}\left[\frac{\tilde{F}(\rho)C_\rho^\eta + \tilde{F}(\theta)C_\theta^\eta + \tilde{F}(\phi)C_\phi^\eta}{J^2}\right]_{\zeta=0} \\ R_1 &= -\frac{1}{J}\left[\frac{\tilde{F}(\rho)C_\rho^\zeta + \tilde{F}(\theta)C_\theta^\zeta + \tilde{F}(\phi)C_\phi^\zeta}{J^2}\right]_{\zeta=0} \end{aligned}\right\} \tag{10}$$

Now, the problem to determine P, Q, and R has been reduced to the problem of evaluating the right-hand side of equation (6) so that three constraints are satisfied.

Since the ξ- and η-derivatives at the body surface can be specified from the body geometry, only the terms including ζ-derivatives are unknowns. They are ρ_ζ, θ_ζ, ϕ_ζ, $\rho_{\zeta\zeta}$, $\theta_{\zeta\zeta}$, and $\phi_{\zeta\zeta}$. Second derivatives are evaluated by the following expressions (see ref. 4):

$$\left.\begin{aligned} \rho_{\zeta\zeta} &= \frac{-7\rho_1 + 8\rho_2 - \rho_3}{2(\Delta\zeta)^2} - \frac{3\rho_\zeta\big|_{\zeta=0}}{(\Delta\zeta)} \\ \theta_{\zeta\zeta} &= \frac{-7\theta_1 + 8\theta_2 - \theta_3}{2(\Delta\zeta)^2} - \frac{3\theta_\zeta\big|_{\zeta=0}}{(\Delta\zeta)} \\ \phi_{\zeta\zeta} &= \frac{-7\phi_1 + 8\phi_2 - \phi_3}{2(\Delta\zeta)^2} - \frac{3\phi_\zeta\big|_{\zeta=0}}{(\Delta\zeta)} \end{aligned}\right\} \tag{11}$$

where subscripts 1, 2, and 3 indicate the indices in the ζ-direction (see fig. 2). If the first terms in equation (1) are evaluated in the previous solution step, then the unknowns to be determined have been reduced to ρ_ζ, θ_ζ, and ϕ_ζ, which can be specified in advance from the constraints described above.

Since instabilities can result if the specified values of ρ_ζ, θ_ζ, and ϕ_ζ are used, the computed values of P, Q, and R are damped in the same way as in ref. 4. In each solution step of the ADI scheme, P (for instance) is evaluated as

$$P_1^{(n+1)} = P_1^{(n)} + \mathrm{SIGN}\left\{\mathrm{MIN}\left[\omega_p\left|P - P^{(n)}\right|,\ P_{Lim}\cdot\mathrm{MAX}(\left|P^n\right|,1)\right],\ P - P^{(n)}\right\} \tag{12}$$

where the superscript indicates the number of the iteration and where ω_p is the underrelaxation parameter. The same procedure is used for Q and R.

Equation (2) is solved by the ADI scheme with the source-term evaluation process shown above. Since the ADI scheme is widely used as a solution method for elliptic equations, the details are not shown here. A false time-step is introduced and the solution of the original elliptic equation is obtained as the time-asymptotic steady-state solution.

APPLICATION TO THE GENERATION OF WARPED SPHERICAL COORDINATES

The essential idea of the transformation between the physical and computational space is shown schematically in figure 1. Bilateral symmetry is imposed, so that the grid is generated in a half-volume. At the axis, on the body boundary, and on the outer boundary, ρ, θ, and ϕ values are specified. At the outflow boundary, ρ, θ, and ϕ are extrapolated so that $\partial x/\partial \eta = 0$ and $\partial y/\partial \eta = 0$ are satisfied in specified z = constant plane.

Since convergence difficulties arose in the ADI solution process, the following optional modifications were included in the program code. First, time-steps can be varied for each of the three equations in equation (3), for small time-steps are required for the ρ-equation in the initial stage of the solution process. Second, the ρ-transformation can be introduced to overcome the trouble appearing near the origin when the origin is chosen to be near the body surface. The orthogonality condition is distorted to some extent when this transformation is introduced. Third, the grid can be redistributed in the ζ-direction. Because stable computations for the very small spacing near the body were difficult, the computations are done for the relatively larger spacing near the body surface, and only grid lines in the ζ-direction are kept. Then, the grid points are redistributed from the body surface to the outer boundary along the obtained ζ-lines. This process makes it possible to obtain Euler and thin-layer Navier-Stokes grids by a single run of the grid-generation program.

It should be noticed that the location of the origin changes the convergence history very much in the present method, using spherical variables, whereas the origin location does not matter when the Cartesian variables are used.

With all these modifications, small time-steps had to be used to avoid the instabilities, and, as a result, convergence was slow and required premature termination of the iteration process before the convergence criterion was satisfied. Thus, the grids obtained are not strictly normal to the body surface but are adequate for the flow-field computations, as is seen in the illustrative examples.

ILLUSTRATIVE EXAMPLES

Examples of the application of this program code to a wide variety of body shapes are presented below. The grid over the body and the outer boundary are given as boundary conditions, and the initial guess for the inner region grid is straight lines for connecting these two boundaries in all the cases presented here.

Hemisphere-Cylinder

The first example is the application of the code to the hemisphere-cylinder. Since the body is axisymmetric, the grid generation is rather easy in this example. In figure 3, the body shape, as well as the computed grid distribution, is presented. The number of grid points is 24 along the axis, 21 in the circumferential direction, and 21 in the radial direction. Stretching of the body-grid spacing is introduced in the η-direction so that the grid obtained can be practically used. Since ϕ values are the same for each ξ = constant plane, it is not necessary to solve the

ϕ-equation, even though the equation is actually solved together. This figure includes $J = 2$, $J = 20$, and $K = 24$ grid surfaces, as well as the body grid.

The redistributed grid, adequate for viscous computations, is shown in figure 4(a), and the blown-up view of ξ-plane grid is shown in figure 4(b). The number of the grid surface in the radial direction is changed from 21 to 31 in this viscous grid. The result indicates that the grid obtained is smooth, and the orthogonality is almost satisfied in this example.

Delta Wing without Trailing Edge

The body shape (fig. 5) is composed of the wing region and the following slab region, which is attached to avoid the expected difficulty associated with the wake treatment. The number of grid points in this example is 31 in the chordwise direction, 31 in the circumferential direction, and 21 from the body to the outer boundary.

Figure 6 shows the overall view of the grid distribution where the $J = 2$, $J = 16$, and $K = 31$ planes are shown, as well as the body grid. Since the focus is on the wing region, a very large stretching ratio for the slab region is used in the chordwise direction. The grid distribution is obtained only for the forward part of the body, and the following grid is obtained by extrapolation, keeping only y and z data from the last computed grid plane in the η-direction. This is done in order to save computer time and avoid instability.

The redistributed viscous grid that was actually used for the thin-layer Navier-Stokes computations (ref. 11) for the leading-edge-separation vortex study is shown in figure 7(a). Close-up views from the front and the top are also shown in figures 7(b) and 7(c). Figure 7(b) is the top view of $J = 2$, $J = 16$ grid surfaces and body grid. Figure 7(c), the view from the front, shows the $J = 2$, $J = 30$, and $K = 15$ surfaces, as well as the body grid. It should be remembered that the $K = 15$ crossflow plane is not a true plane but a curved surface bending toward the front, as is seen in figure 7(a). The origin was taken to be the apex of the body, and thus the weak ρ-transformation was introduced in this example. These figures indicate that the grid is not strictly orthogonal, but that it is adequate for the flow-field computations. The grid distribution caused no troubles throughout the flow-field computations. Much clustering and stretching is used on the boundary in both the ξ- and η-directions to make the grid useful for the flow-field computation. Thus, the computation of the grid distribution in this case is not as easy as the computation for the constantly distributed body-grid case.

Space Shuttle Geometry

The present method was applied to the complicated geometry of the Space Shuttle. The body shape is given by the geometry package called "GEOM3." Complete details of the geometry package used here are given in reference 12. The body grid is obtained by cubic-spline interpolation, so that the grid is clustered near the wing-tip region, etc. The number of grid points is 38 in the chordwise direction, 51 in the circumferential direction, and 31 from the body to the outer boundary. This is almost the maximum number of grid points used for the flow-field computations, using the

vectorized version of the thin-layer Navier-Stokes solution code.[2] Because of this limitation, the wing region does not have enough points in the chordwise direction. A grid having 46 points in the chordwise direction was also generated and showed a very similar result.

Figure 8 shows the geometry and the body grid. The distribution of the grid points over the geometry is performed by using an interactive grid-distribution program including a display capability. Figure 9(a) shows the overall view of the viscous grid, where $j = 2$, $j = 50$, and $k = 38$ planes are seen. Figures 10(a)-10(d) show the view of the crossflow grid from the front. Again, it should be remembered that these are not planes but curved surfaces. In each figure, the grid orthogonality is not satisfied but the grid is acceptable. The grid distribution is smooth, even in the region of wing-body junction where grid generation might be very difficult.

CONCLUSIONS

A grid-generation program code has been developed for three-dimensional geometries. In this code, spherical variables were used to avoid the axis-singularity problem, and a set of three-dimensional Poisson equations was solved by the ADI scheme. The orthogonality condition and the minimum spacing restriction on the body surface were imposed as source terms in the equations. The program code was written for generating the warped spherical coordinate system, but can be easily extended to other topologies.

The program code was applied to several geometries, and the results indicate that it can generate a grid that is adequate for the flow-field computations, even though the strict orthogonality was not satisfied.

[2]The original program code was capable of using only half this number of points. A modification of the program was made by the present author, and this number of grid points for the flow-field computations became possible using the Solid State Disk Device (SSD) on the CRAY 1-S.

APPENDIX

APPLICATION OF THE PRESENT METHOD TO THE THIN, DELTA WING

The present code was applied to generate the warped spherical coordinate system over a thin, delta wing. Since generating thin, sometimes zero-thickness, body geometry is very difficult, the following procedure is used. First, the grid distribution is done for a thicker wing having no trailing-edge. The grid-generation process is the same as that used in the delta wing example above. The body grid for the thin wing, which has zero thickness in the wake region, is distributed so that the spacing ratio in both the ξ- and η-directions are the same as for the thicker wing. Then, each ζ-line for the thicker body is extended to the corresponding thin-body grid; ζ-lines are smoothly redistributed, using cubic-spline interpolation. A typical crossflow plane grid in the wing region is shown in figure 11; figure 12 shows the grid in the wake region. Since the body is very thin, the orthogonality is not much distorted by the process above. The flow-field computations were actually done and were successful. In this topology, the transformation Jacobian becomes singular along the line starting at the wing tip in the wake region. This was overcome by special treatment of that line.

REFERENCES

1. Kutler, P.: A Perspective of Theoretical and Applied Computational Fluid Dynamics. AIAA Paper 83-0037, Reno, Nev., 1983.

2. Thompson, J. F.; Thames, F. C.; and Mastin, C. W.: Automatic Numerical Generation of a Body-Fitted Curvilinear Coordinate System for Field Containing Any Number of Arbitrary Two-Dimensional Bodies. J. Comp. Phys., vol. 15, 1974, pp. 299-319.

3. Steger, J. L.; and Sorenson, R. L.: Automatic Mesh-Point Clustering near a Boundary in Grid Generation with Elliptic Partial Differential Equations. J. Comp. Phys., vol. 33, 1979, pp. 405-410.

4. Sorenson, R. L.: A Computer Program to Generate Two-Dimensional Grids about an Airfoil and Other Shapes by the Use of Poisson's Equations. NASA TM-81,198, 1980.

5. Chyu, W. J.; Davis, S. S.; and Chang, K. S.: Calculation of Unsteady Transonic Flow over an Airfoil. AIAA J., vol. 19, no. 6, June 1981.

6. Lasinski, T. A.; Andrews, A. E.; Sorenson, R. L.; Chaussee, D. S.; and Kutler, P.: Computation of the Steady Viscous Flow over a Tri-Element "Augmentor Wing" Airfoil. AIAA Paper 82-0021, 1982.

7. Van Dalsem, W. R.; and Steger, J. L.: Finite-Difference Simulation of Transonic Separated Flow Using a Full Potential-Boundary Layer Interaction Approach. AIAA Paper 83-1689, Danvers, Mass., 1983.

8. Thomas, P. D.: Composite Three Dimensional Grids Generated by Elliptic System. AIAA J., vol. 20, no. 9, Sept. 1982.

9. Shieh, C. F.: Three-Dimensional Grid Generation Using Elliptic Equations with Direct Grid Distribution Control. AIAA Paper 83-0448, Reno, Nev., 1983.

10. Sorenson, R. L.; and Steger, J. L.: Grid Generation in Three Dimensions by Poisson Equations with Control of Cell Size and Skewness at Boundary Surfaces. Mini-Symposium on Advances in Grid Generation, ASME Fluid Engineering Conference, Houston, Tex., June 1983.

11. Fujii, K.; and Kutler, P.: Numerical Simulation of the Leading-Edge Separation Vortex for a Wing and Strake-Wing Configuration. AIAA Paper 83-1908, Danvers, Mass., 1983.

12. Kutler, P.; Reinhardt, W. A.; and Warming, R. F.: Multishocked, Three-Dimensional Supersonic Flowfields with Real Gas Effects. AIAA J., vol. 11, May 1973, pp. 657-664.

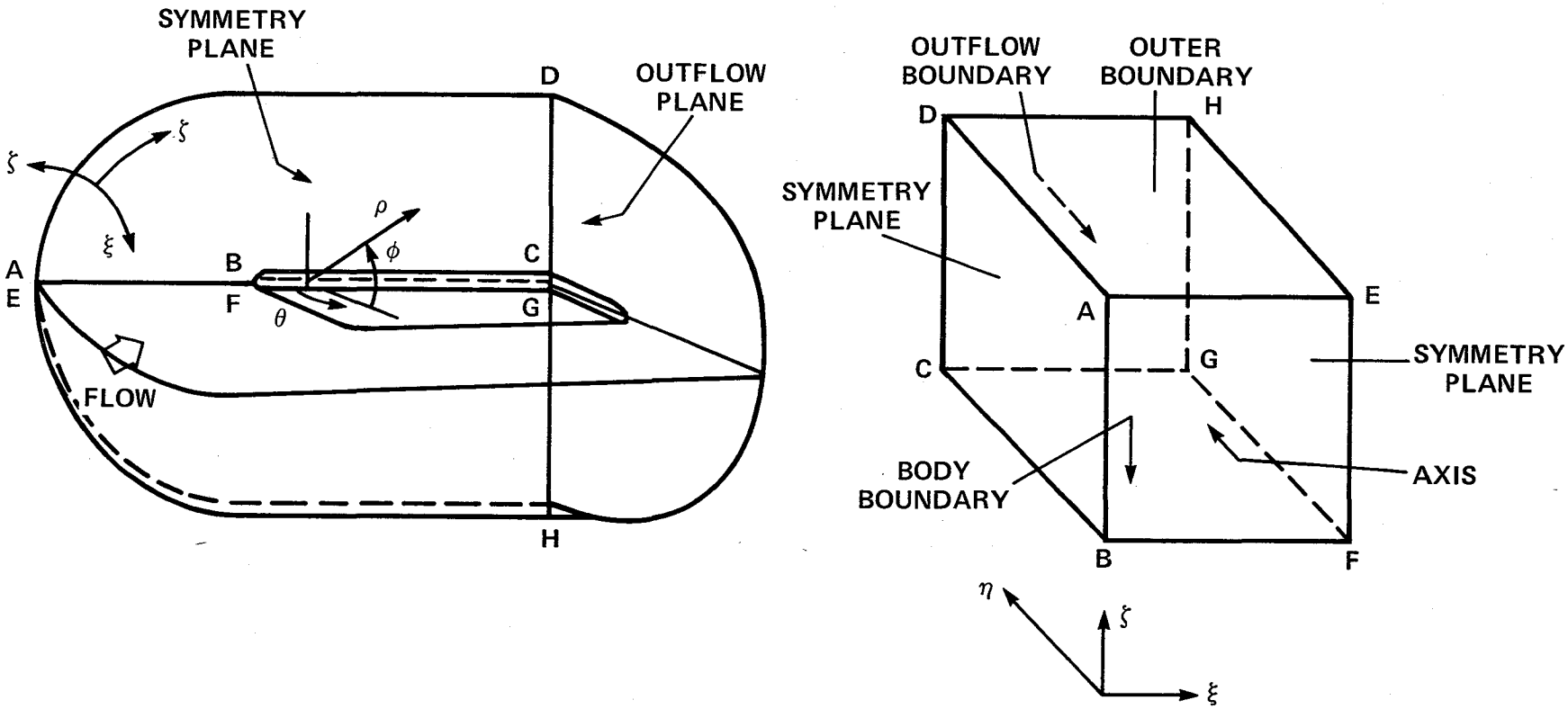

(a) Physical space.

(b) Computational space.

Figure 1.- Correspondence between physical space and computational space.

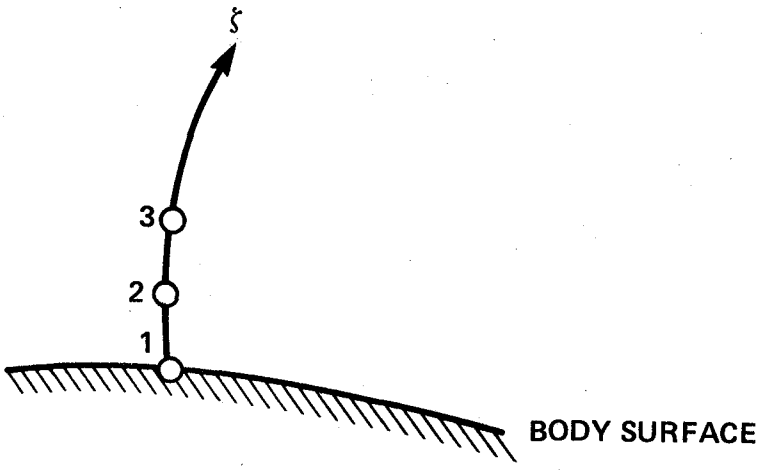

Figure 2.- Grid near the body surface.

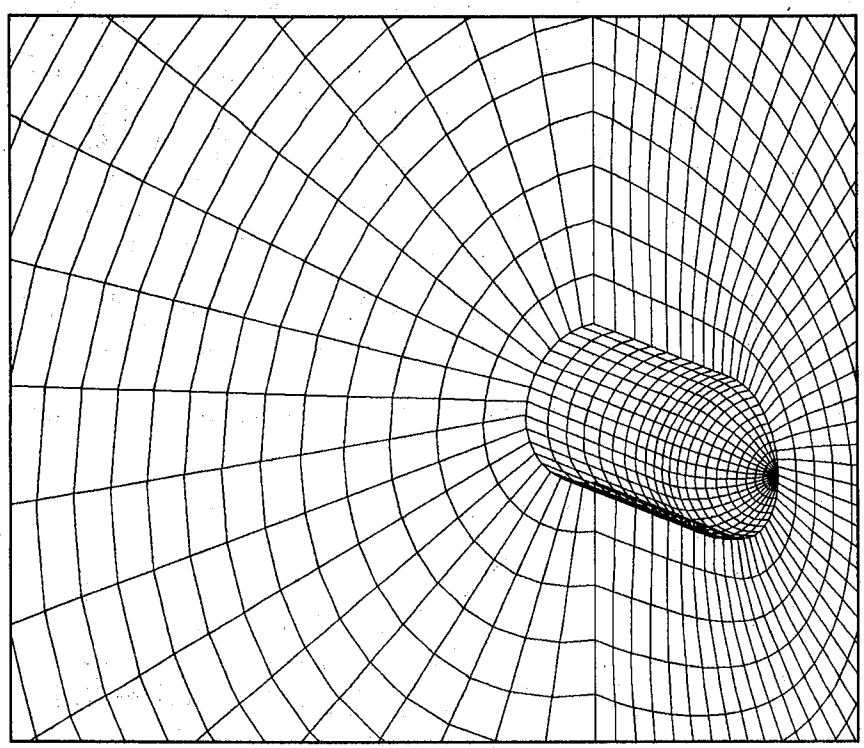

Figure 3.- Grid over hemisphere-cylinder.

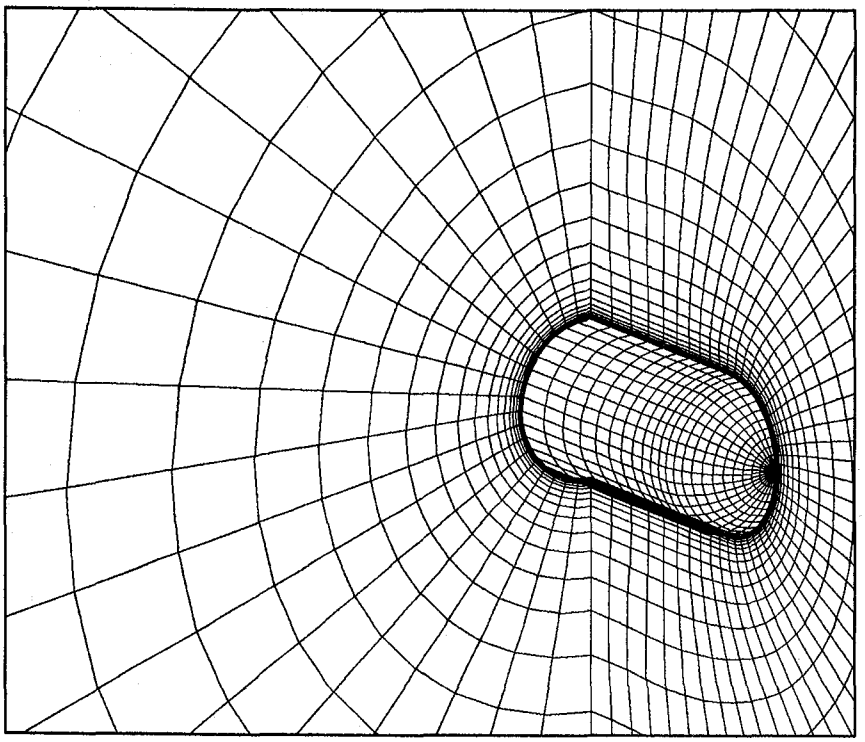

(a) Redistributed viscous grid over hemisphere-cylinder.

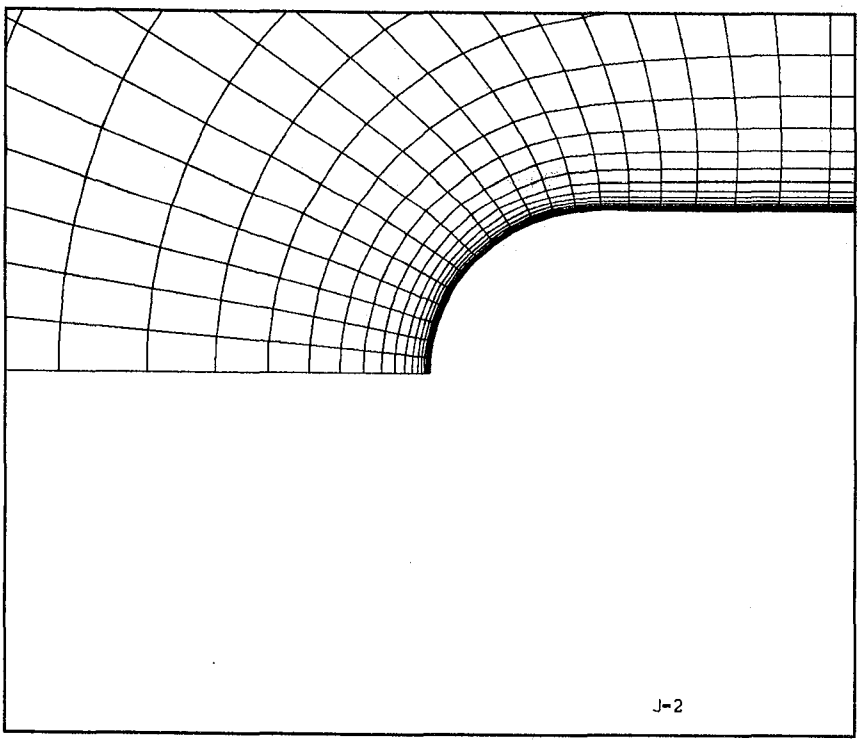

(b) Close-up view of ξ-plane grid.

Figure 4.- Grid over hemisphere-cylinder for viscous flow computations.

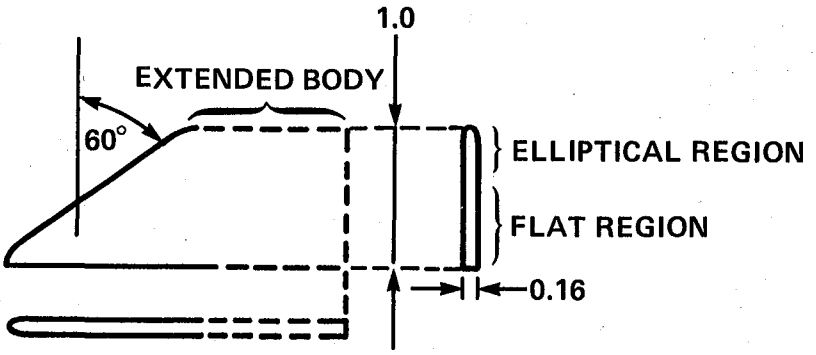

Figure 5.- Body geometry.

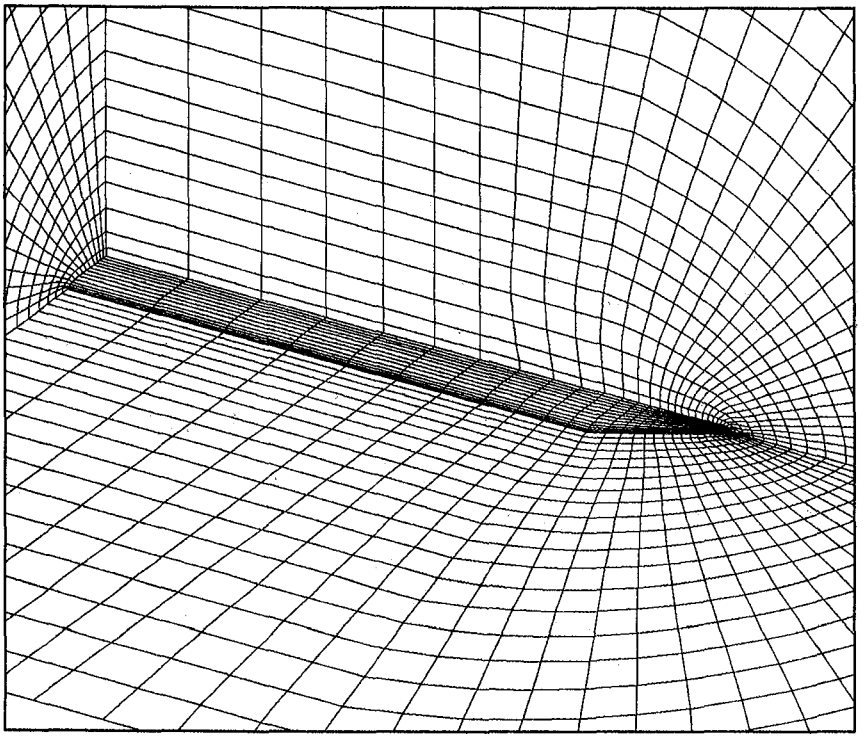

Figure 6.- Overall view of the grid.

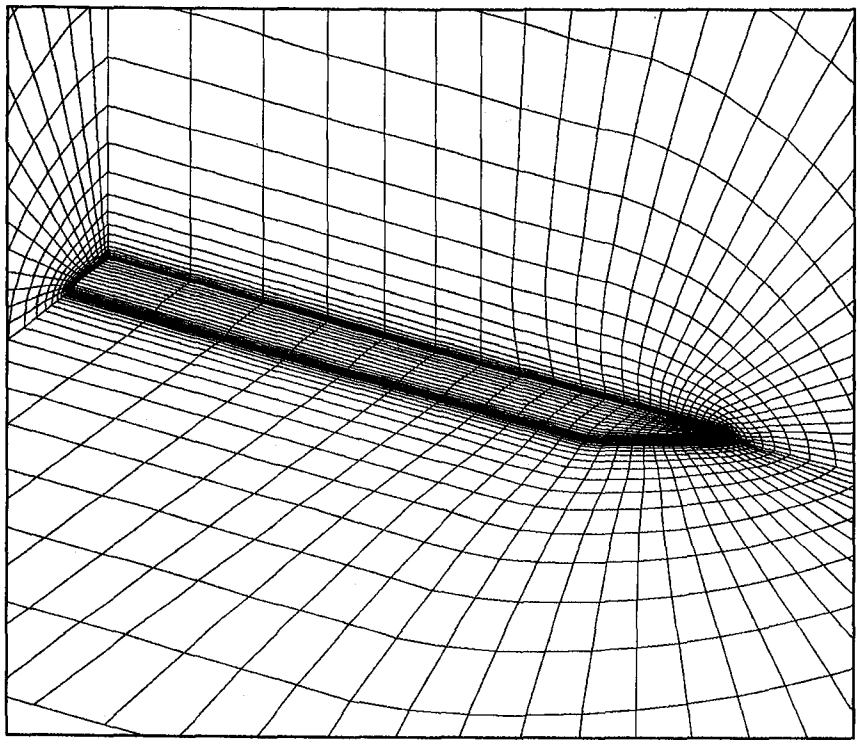

(a) Overall view of the redistributed viscous grid.

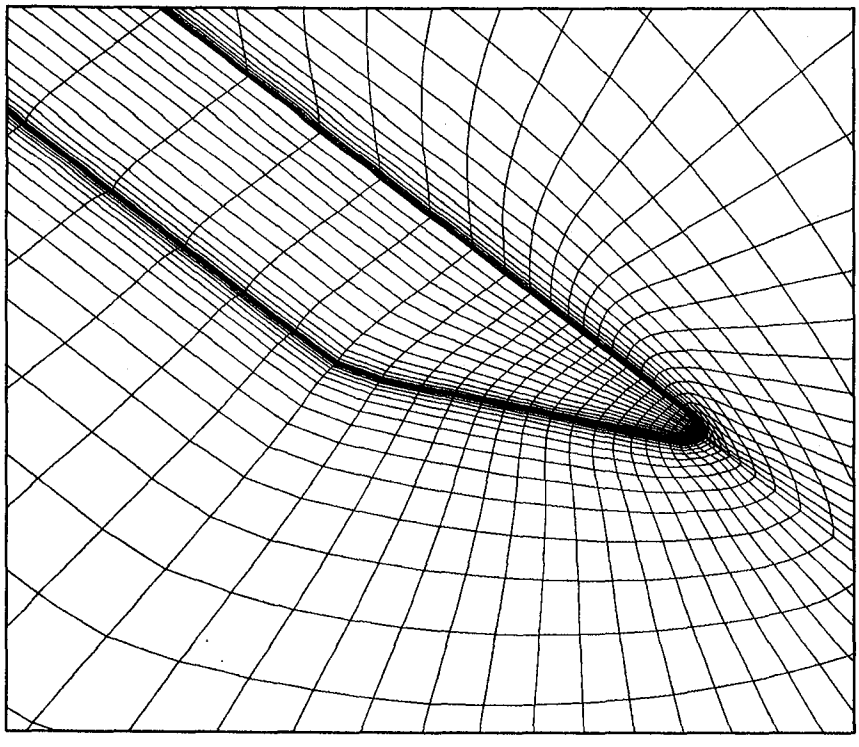

(b) Close-up view of the grid from the top.

Figure 7.- Grid over delta wing for viscous flow computations.

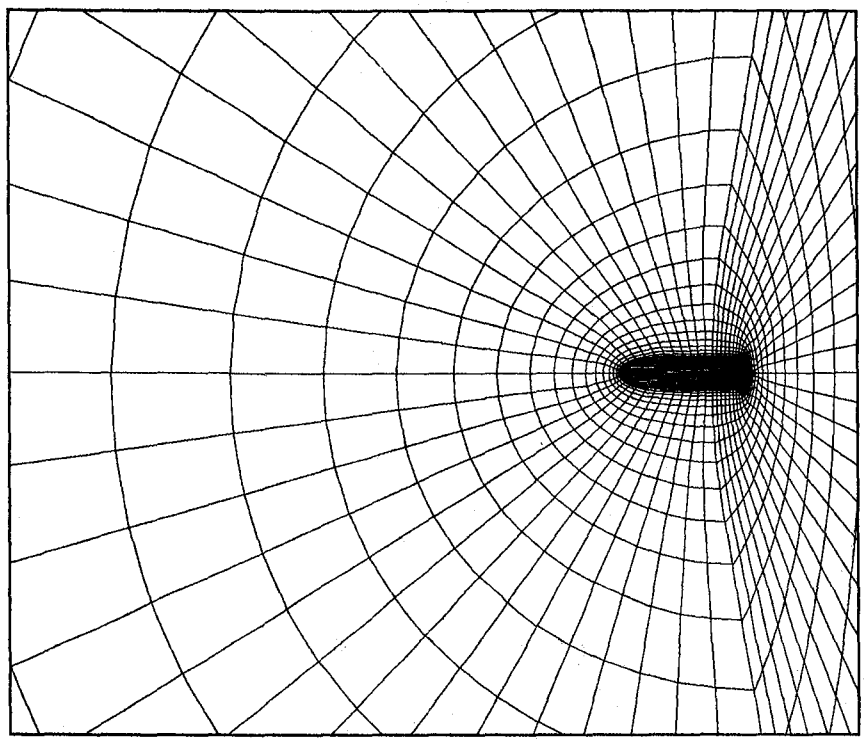

(c) Close-up view of the grid from the front.

Figure 7.- Concluded.

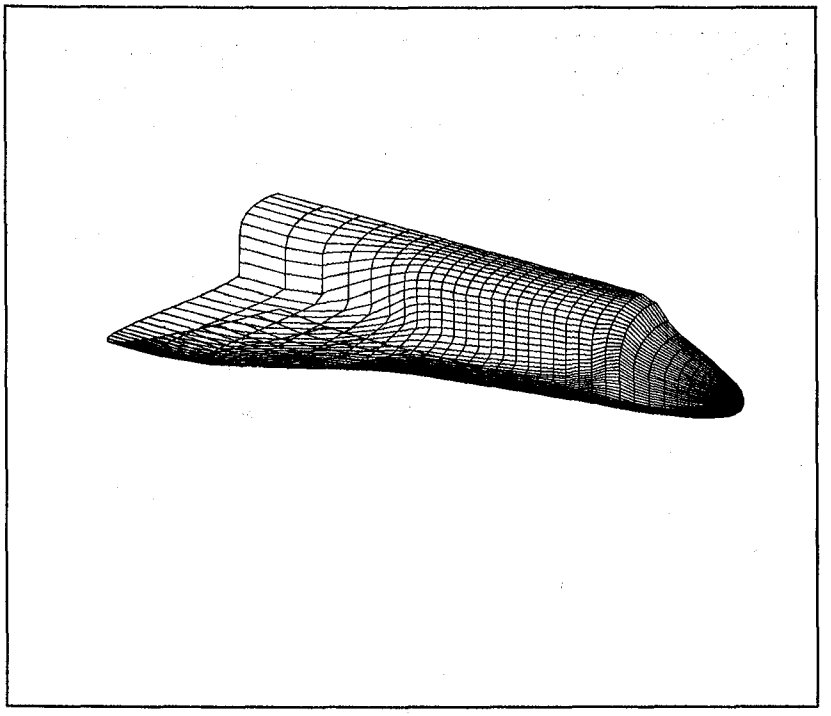

Figure 8.- Shuttle geometry and the body grid.

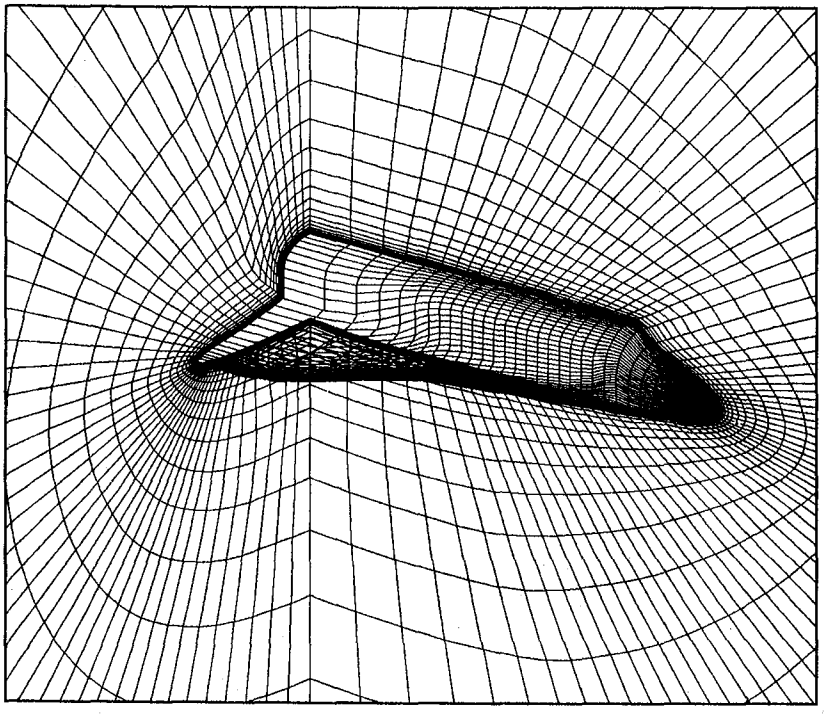

Figure 9.- Overall view of the grid (redistributed for the viscous computations).

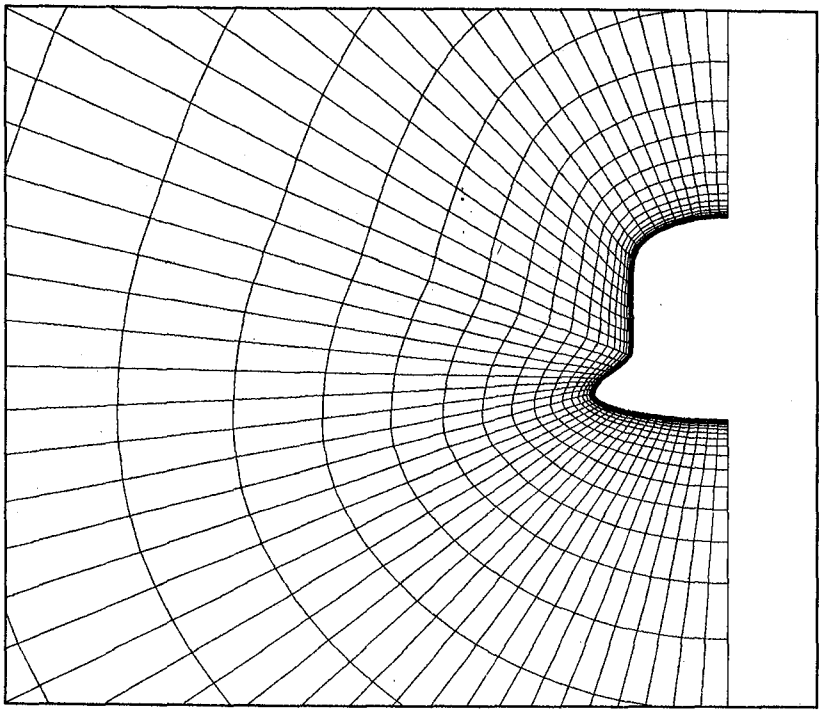

(a) K = 25.

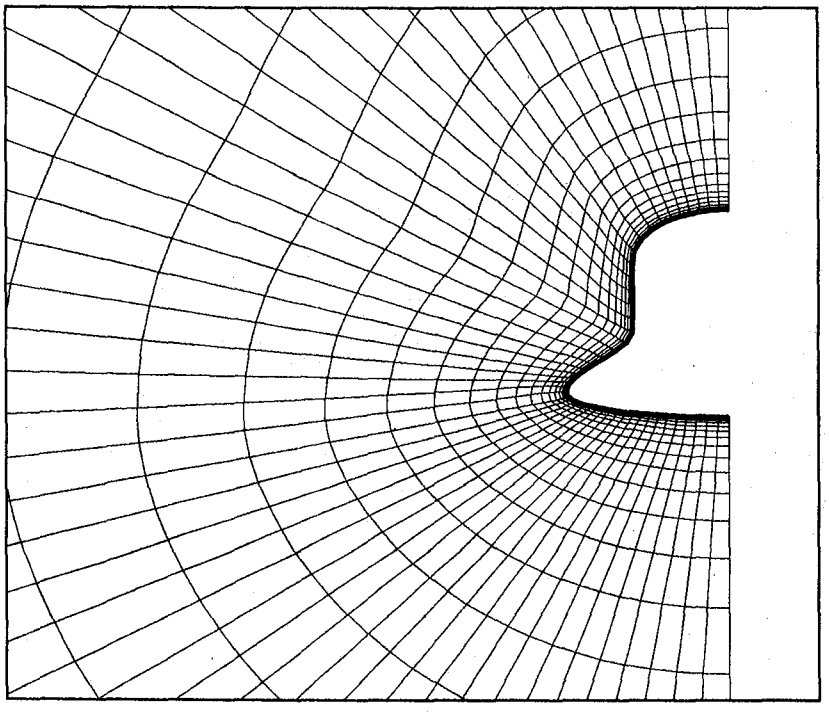

(b) K = 30.

Figure 10.- Close-up view of the crossflow plane grid.

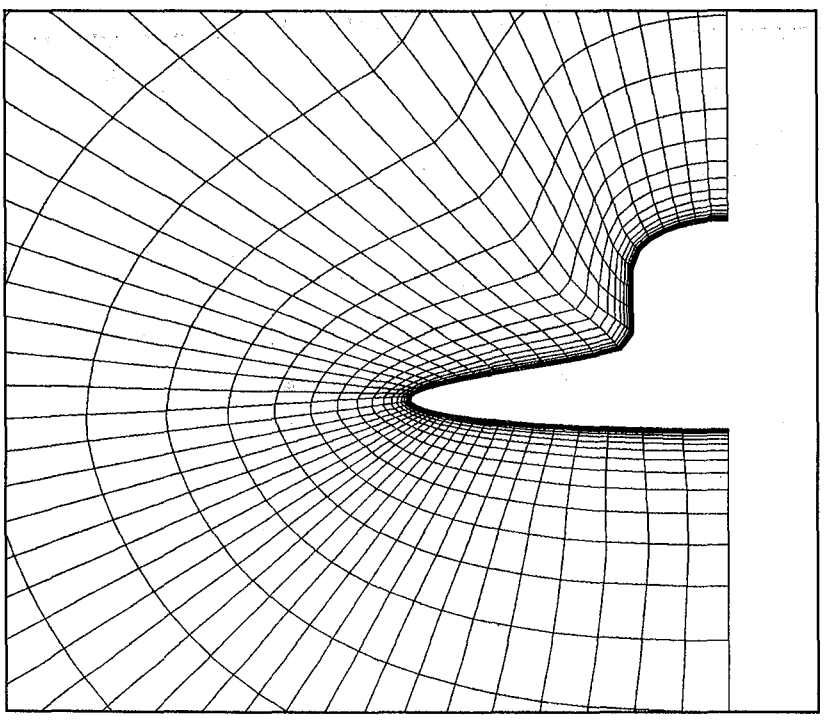

(c) K = 35.

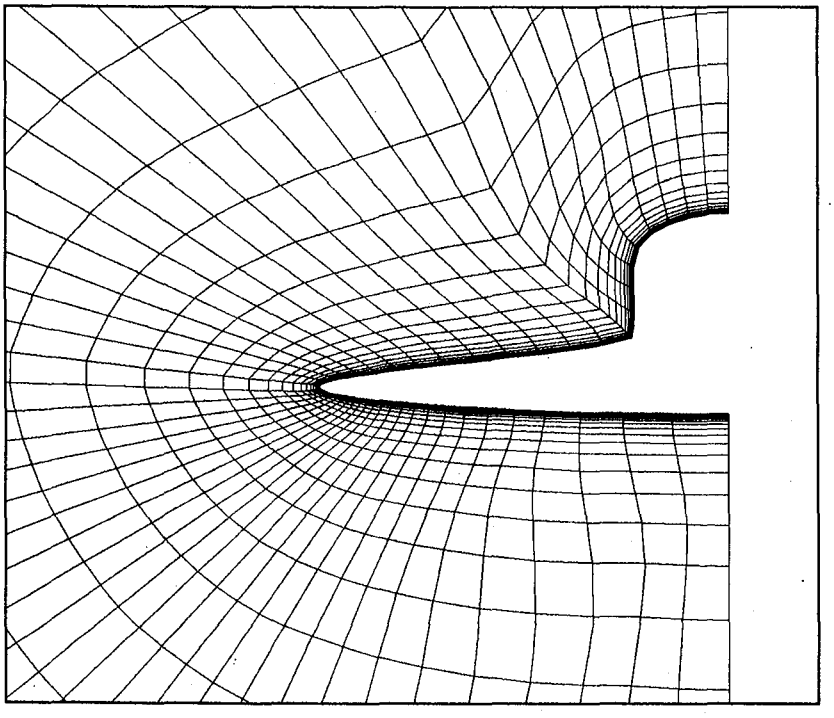

(d) K = 38.

Figure 10.- Concluded.

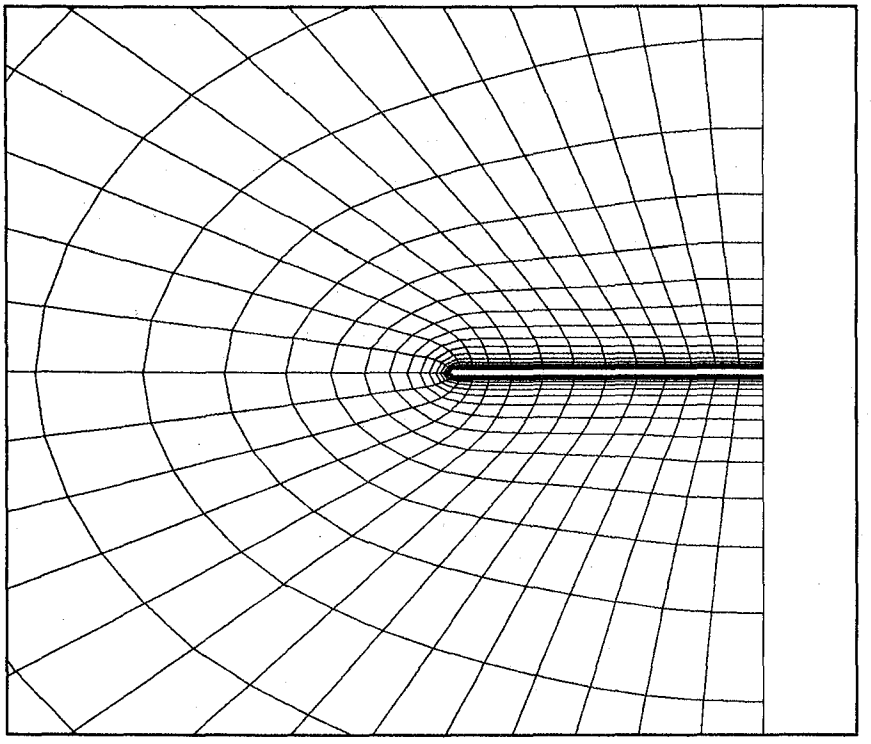

Figure 11.- Crossflow surface grid for thin wing (wing region).

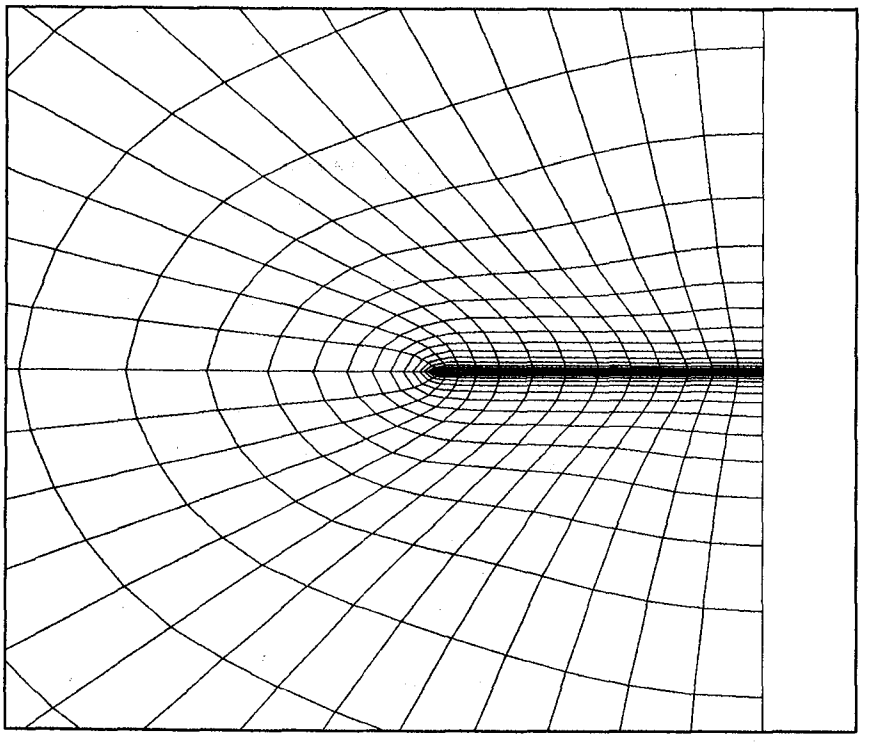

Figure 12.- Crossflow surface grid for thin wing (wake region).

1. Report No.	2. Government Accession No.	3. Recipient's Catalog No.
NASA TM-85857		

4. Title and Subtitle	5. Report Date
SOLUTION OF POISSON EQUATIONS FOR THREE-DIMENSIONAL GRID GENERATIONS	October 1983
	6. Performing Organization Code
7. Author(s)	8. Performing Organization Report No.
K. Fujii	A-9527
	10. Work Unit No.
9. Performing Organization Name and Address	T-6457
NASA Ames Research Center Moffett Field, Calif. 94035	11. Contract or Grant No.
	13. Type of Report and Period Covered
12. Sponsoring Agency Name and Address	Technical Memorandum
National Aeronautics and Space Administration Washington, D.C. 20546	14. Sponsoring Agency Code
	505-31-01-01-00

15. Supplementary Notes

Point of contact: P. Kutler, Ames Research Center, M/S 202A-14, Moffett Field, Calif. 94035, (415)965-6032 or FTS 448-6032

16. Abstract

A method for generating three-dimensional, finite-difference grids about complicated geometries by using Poisson equations is developed. The inhomogeneous terms are automatically chosen such that orthogonality and spacing restrictions at the body surface are satisfied. Spherical variables are used to avoid the axis singularity, and an alternating-direction-implicit (ADI) solution scheme is used to accelerate the computations. Computed results are presented that show the capability of the present method. Since most of the results presented in this paper have been used as grids for flow-field computations, this is indicative that the present method is a useful tool for generating three-dimensional grids about complicated geometries.

17. Key Words (Suggested by Author(s))	18. Distribution Statement
Grid generation Numerical methods	Unlimited Subject Category - 64

19. Security Classif. (of this report)	20. Security Classif. (of this page)	21. No. of Pages	22. Price*
Unclassified	Unclassified	25	A02

*For sale by the National Technical Information Service, Springfield, Virginia 22161